

Proper motion L and T dwarf candidate members of the Pleiades

S. L. Casewell¹*, P. D. Dobbie^{1,2}, S. T. Hodgkin³, E. Moraux⁴, R. F. Jameson¹,
 N. C. Hambly⁵, J. Irwin³ and N. Lodieu^{6,1}

¹Department of Physics and Astronomy, University of Leicester, University Road, Leicester LE1 7RH, UK

²Anglo-Australian Observatory, PO Box 296, Epping NSW 1710 Australia

³CASU, Institute of Astronomy, University of Cambridge, Madingley Road, Cambridge, CB3 0HA, UK

⁴Laboratoire d’Astrophysique, Observatoire de Grenoble, Université Joseph Fourier, BP 53, 38041 Grenoble Cedex 9, France

⁵Scottish Universities Physics Alliance (SUPA), Institute for Astronomy, School of Physics, University of Edinburgh,

Royal Observatory, Blackford Hill, Edinburgh EH9 3HJ

⁶Instituto de Astrofísica de Canarias, Vía Láctea s/n, E-38205 La Laguna, Tenerife, Spain

January 2007

ABSTRACT

We present the results of a deep optical-near-infrared multi-epoch survey covering 2.5 square degrees of the Pleiades open star cluster to search for new very-low-mass brown dwarf members. A significant (~ 5 year) epoch difference exists between the optical (CFH12k I -, Z -band) and near infrared (UKIRT WFCAM J -band) observations. We construct I, I - Z and Z, Z - J colour magnitude diagrams to select candidate cluster members. Proper motions are computed for all candidate members and compared to the background field objects to further refine the sample. We recover all known cluster members within the area of our survey. In addition, we have discovered 9 new candidate brown dwarf cluster members. The 7 faintest candidates have red Z - J colours and show blue near-infrared colours. These are consistent with being L and T-type Pleiads. Theoretical models predict their masses to be around $11M_{\text{Jup}}$.

Key words: stars: low-mass, brown dwarfs, open clusters and associations: individual:Pleiades

1 INTRODUCTION

The initial mass spectrum (IMS), the number of objects manufactured per unit mass interval, is an outcome of the star formation process which can be constrained via observation. Consequently, empirical determinations of the form of the IMS can be used to critically examine our theoretical understanding of the complexities of star formation. In recent years there has been a particular emphasis on building a solid comprehension of the mechanisms by which very-low-mass stars, brown dwarfs and free-floating planetary mass objects form (e.g. Boss 2001; Bate 2004; Goodwin, Whitworth & Ward-Thompson 2004; Whitworth & Goodwin 2005). Nevertheless, one key question which remains unanswered is what is the lowest possible mass of object that can be manufactured by the star formation process? From a theoretical stance, traditional models predict that if substellar objects form like stars, via the fragmentation and collapse of molecular clouds, then there is a strict lower mass limit to their manufacture of 0.007 - $0.010 M_{\odot}$ (Padoa & Nordlund, 2002). This is set by the rate at which the gas can radiate away the heat released by the compression (e.g. Low & Lynden-Bell, 1976). However, in more elaborate theories, magnetic fields could cause rebounds in collapsing cloud cores which might lead

to the decompressional cooling of the primordial gas, a lowering of the Jeans mass and hence the production of gravitationally bound fragments with masses of only $\sim 0.001 M_{\odot}$ (Boss, 2001). In contrast, if feedback from putative winds and outflows driven by the onset of deuterium burning play a role, the smallest objects which form via the star formation process may be restricted to masses equal to or greater than the deuterium burning limit ($\sim 0.013 M_{\odot}$; Adams & Fatuzzo, 1996).

Recent work on very young clusters ($\tau < 10$ Myrs) and star formation regions e.g. σ -Orionis, the Trapezium, IC348 and Upper Sco (Béjar et al., 2001; Muench et al., 2002; Muench et al., 2003; Lodieu et al., 2007a) suggests that the initial mass function continues slowly rising down to masses of the order $M \sim 0.01 M_{\odot}$, at least in these environments. Indeed, it has been claimed that an object with a mass as low as 2 - $3 M_{\text{Jup}}$ has been unearthed in σ -Ori (Zapatero-Osorio et al., 2002). However, the cluster membership of σ -Ori 70 is disputed by Burgasser et al. (2004). Furthermore, mass estimates for such young substellar objects derived by comparing their observed properties to the predictions of theoretical evolutionary tracks remain somewhat controversial. Baraffe et al. (2002) have shown that to robustly model the effective temperature and luminosity of a low mass object with an age less than ~ 1 Myr, evolutionary calculations need to be coupled to detailed simulations of the collapse and accretion phase of star formation.

* E-mail: slc25@star.le.ac.uk

As the current generation of evolutionary models start from arbitrary initial conditions, theoretical predictions for ages less than a few Myrs must be treated with a fair degree of caution. Indeed, the few available dynamical mass measurements of pre-main sequence objects indicate that models tend to underestimate mass by a few tens of percent in the range $0.3 \lesssim M \lesssim 1.0 M_{\odot}$ (see Hillenbrand & White, 2004 for review). A recent dynamical mass measurement of the 50-125 Myrs old object AB Dor C (spectral type $\sim M8$), the first for a pre-main sequence object with $M < 0.3 M_{\odot}$, suggests that the discrepancy between model predictions and reality might be even larger at lower masses, with the former underestimating mass by a factor 2-3 at $M \sim 0.1 M_{\odot}$ (Close et al., 2005). However, this conclusion is dependent on the assumed age of AB Dor, which is currently a matter of great contention (Luhman, Stauffer & Mamajek, 2005; Janson et al., 2006). On the positive side, Zapatero-Osorio et al., (2004) have determined the masses of the brown dwarf binary components of GJ 569 Bab and their luminosities and effective temperatures are in agreement with theoretical predictions, for an age of 300 Myr. More recently, Stassun, Mathieu & Valenti (2006) discuss an eclipsing brown dwarf binary in the Orion nebula star forming region and find the large radii predicted by theory for a very young dwarf. Surprisingly, they find that the secondary is hotter than the more massive primary. Clearly further work is still needed to support the predictions of theoretical models.

It is clearly important to search for the lowest mass objects, not only in the young clusters, but also in more mature clusters, such as the Pleiades. The results of previous surveys of the Pleiades indicate that the present day cluster mass function, across the stellar/substellar boundary and down to $M \sim 0.02 M_{\odot}$ (based on the evolutionary models of the Lyon Group), can be represented by a slowly rising power law model, $dN/dM \propto M^{-\alpha}$. For example, from their Canada-France-Hawaii Telescope (CFHT) survey conducted at *R* and *I* and covering 2.5 sq. degrees, Bouvier et al. (1998) identified 17 candidate brown dwarfs ($I_C \geq 17.8$) and derived a power law index of $\alpha = 0.6$. From their 1.1 sq degrees Isaac Newton Telescope (INT) survey conducted at *I* and *Z*, with follow-up work undertaken at *K*, Dobbie et al. (2002) unearthed 16 candidate substellar members and found a power law of index $\alpha = 0.8$ to be compatible with their data. Jameson et al. (2002) showed that a powerlaw of index $\alpha = 0.41 \pm 0.08$ was consistent with the observed mass function over the range $0.3 \gtrsim M \gtrsim 0.035 M_{\odot}$. This study used a sample of 49 probable brown dwarf members assembled from the four most extensive CCD surveys of the cluster available at the time, the International Time Project survey (Zapatero Osorio et al., 1998), the CFHT survey (Bouvier et al., 1998; Moraux, Bouvier & Stauffer, 2001), the Burrell Schmidt survey (Pinfield et al., 2000) and the INT survey (Dobbie et al., 2002). The CFHT survey was subsequently extended to an area of 6.4 sq. degrees (at *I* and *Z*) and unearthed a total of 40 candidate brown dwarfs. Moraux et al. (2003) applied statistical arguments to account for non-members in their sample and derived a power law index of $\alpha = 0.6$. Most recently, Bihain et al. (2006) have used deep *R*, *I*, *J* and *K* band photometry and proper motion measurements to unearth 6 robust L type Pleiades members in an area of 1.8 sq. degrees with masses in the range $0.04-0.02 M_{\odot}$ and derived a power law index of $\alpha = 0.5 \pm 0.2$.

Here we report the results of a new optical/infrared survey of 2.5 sq. degrees of the Pleiades, the aim of which is to extend empirical constraints on the cluster mass function down to the planetary mass regime ($M \sim 0.01 M_{\odot}$). In the next section we describe the observations acquired/used as part for this study, their reduction, their calibration and their photometric completeness. In subsequent sections we describe how we have identified candidate brown dwarf

members on the basis of colours and proper motions. We use our new results to constrain the form of the cluster mass function and conclude by briefly discussing our findings in the context of star formation models.

2 OBSERVATIONS, DATA REDUCTION AND SURVEY COMPLETENESS

2.1 The *J* band imaging and its reduction

Approximately 3.0 square degrees of the Pleiades cluster was observed in the *J* band using the Wide Field Camera (WFCAM) on the United Kingdom Infrared Telescope (UKIRT) between the dates of 29/09/2005 and 08/01/2006. WFCAM is a near infrared imager consisting of 4 Rockwell Hawaii-II (HgCdTe 2048x2048) arrays with $0.4''$ pixels, arranged such that 4 separate pointings (pawprints) can be tiled together to cover a 0.75 sq. degree region of sky (see <http://www.ukidss.org/technical/technical.html> for diagram). A total of four tiles were observed in a mixture of photometric and non-photometric conditions but in seeing of typically ≈ 1.0 arcsecond or better. To ensure that the images were properly sampled we employed the 2×2 microstep mode. The locations on the sky of our tiles (shown in Figure 1) were chosen to provide maximum overlap with the optical fields surveyed in 2000 by the Canada-France-Hawaii telescope and CFH12k camera but also to avoid bright stars and areas of significant interstellar extinction.

The images were reduced at the Cambridge Astronomical Survey Unit (CASU) using procedures which have been custom written for the treatment of WFCAM data. In brief, each frame was debiased, dark corrected and then flat fielded. The individual dithered images were stacked before having an object detection routine run on them. The detection procedure employs a core radius of 5 pixels, and identifies objects as islands of more than 4 interconnected pixels with flux $> 1.5\sigma$ above the background level. The frames were astrometrically calibrated using point sources in the Two micron All Sky Survey (2MASS) catalogue. These solutions, in general, had a scatter of less than 0.1 arcseconds. The photometric calibration employed by the CASU pipeline also relies on 2MASS data (there are typically hundreds of 2MASS calibrators per detector) and is found to be accurate to $\approx 2\%$ in good conditions (see Warren et al., 2007, Hodgkin et al., 2007 for details).

In measuring our photometry we used an aperture of $2''$, which is approximately twice the core radius of point sources. This $2''$ diameter of the aperture is also twice the seeing FWHM. The reduction pipeline also attempts to classify each source depending on its morphology (e.g. galaxy, star, noise). However, at the limit of the data this classification becomes less reliable. Therefore, in our subsequent analysis we chose to define as stellar all objects which lie within 3 sigma of the stellar locus, where sigma is defined according to Irwin et al. (in prep).

2.2 The far-red optical imaging and a new reduction

As part of this work we have used a subset (2.54 square degrees) of the far-red optical data obtained in the course of the *IZ* survey of the Pleiades conducted in 2000 by Moraux et al. (2003). The relevant CFH12k data were extracted from the Canadian Astrophysical Data Center archive and were reprocessed at Cambridge University using the CASU optical imaging pipeline (Irwin & Lewis, 2001). In brief, these data were bias subtracted and corrected for non-linearity prior to flat fielding. Fringe maps, which were constructed

J2000.0

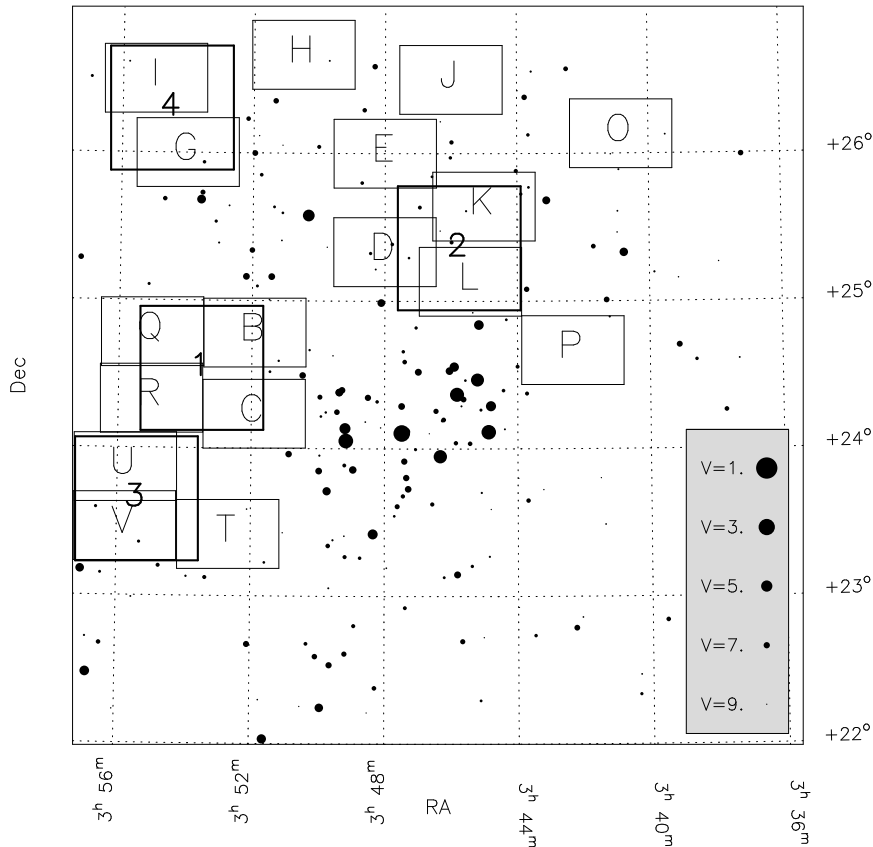


Figure 1. The regions imaged at I , Z and J with the CFHT and UKIRT. The CFH12k pointings (light rectangular outlines) are labelled alphabetically as in Moraux et al. (2003), while the WFCAM tiles (bold square outlines) are labelled numerically, ranging from 1 to 4. Note that the observations avoid the region of high reddening to the south of the Merope and the bright stars in vicinity of the cluster centre.

for each photometric band from images obtained during the observing run, were used to remove the effects of interference between night sky lines in the CCD substrate. Subsequently, sources at a level of significant of 3σ or greater were morphologically classified and aperture photometry obtained for each. A World Coordinate System (WCS) was determined for each frame by cross-correlating these sources with the Automated Plate Measuring (APM) machine catalogue (Irwin, 1985). The approximately 100 common objects per CCD chip lead to an internal accuracy of typically better than $0.3''$. The photometry was calibrated onto a CFH12k I and Z natural system using stars with near zero colour ($B-V-R-I \approx 0$) in Landolt standard field SA98 (Landolt, 1992) which was observed the same nights as the science data. The systematic errors in the photometry were calculated by comparing the photometry of overlapping fields as in Moraux et al. (2003). The photometry was found to be accurate to $\approx 3\%$.

2.3 The completeness of datasets

To estimate the completeness of our IR images, we injected fake stars with magnitudes in the range $J=12-22$ into each of the 16 chips of every WFCAM frame and re-ran the object detection software with the same parameters that were used to detect the real sources. To avoid significantly increasing the density of all sources in the data we inserted only 200 fake stars per chip in a given run. To provide meaningful statistics we repeated this whole procedure

ten times. Subsequently, we calculated percentage completeness at a given magnitude by taking the ratio of the number of fake stars recovered to the number of fake stars injected into a given magnitude bin (and multiplying by 100). We note that a 100% recovery rate was never achieved at any magnitude since a small proportion of the fake stars always fell sufficiently close to other sources to be overlooked by the object detection algorithm. This method was also applied to determine the completeness of the I and Z band CFH12k data. However, the magnitude range of the fake stars was adjusted to be consistent with the different saturation and faint end magnitude limits of these data. The results of this procedure for all 3 photometric bands are shown in Table 1.

A glance at this table indicates that the IR data are in general 90% complete to $J \approx 19.7$, although Field 3 is slightly less deep, due to moonlight and poor seeing. In this case the proximity of the moon led to higher background counts. The I data are typically 90% and 50% complete to $I=22.5$ and 23.5 respectively. The corresponding completeness limits for the Z band data are $Z=21.5$ and 22.5 respectively.

3 ANALYSIS OF THE DATA

3.1 Photometric selection of candidate cluster members

An initial photometrically culled sample of candidate brown dwarfs has been obtained from the $I, I-Z$ colour-magnitude diagram (Fig-

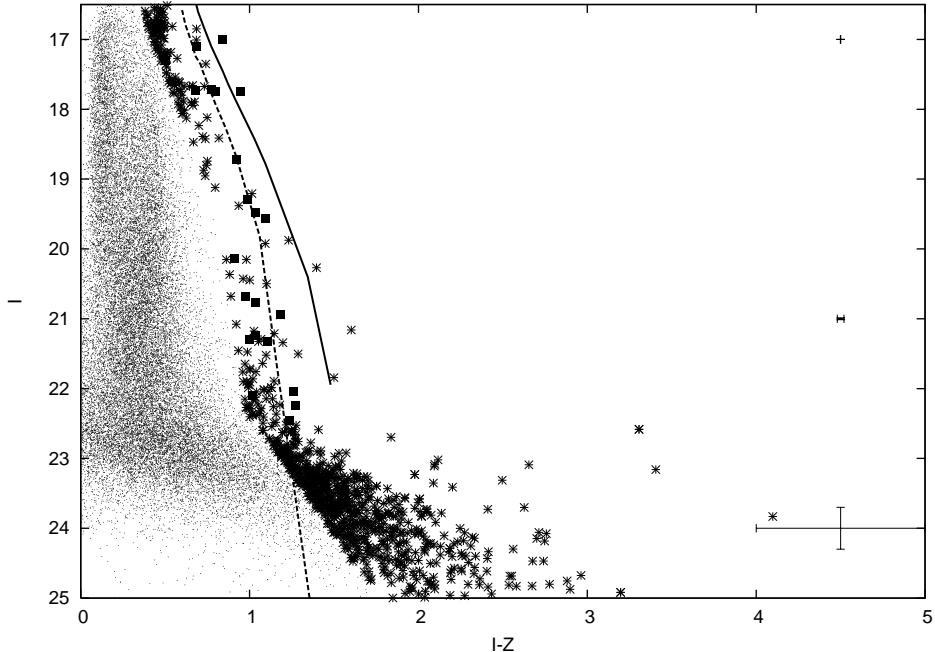


Figure 2. The $I, I-Z$ CMD for the whole of field 1. The solid line is the NEXTGEN model, and the dotted line the DUSTY model. The small points are all objects that were classed as stellar in both I and Z data. The crosses are all objects that met the following selection criteria: classed as stellar in both I and Z data, for $16.5 < I < 22.5$, they must lie no more than 0.25 magnitudes to the left of the DUSTY isochrone, for $I \geq 22.5$, they must lie to the right of the line, $I-Z = (I-19.0)/3.5$. The filled squares are the previously identified cluster candidate members from Bihain et al. (2006), Moraux et al. (2003) and Bouvier et al. (1998), plotted to highlight the cluster sequence.

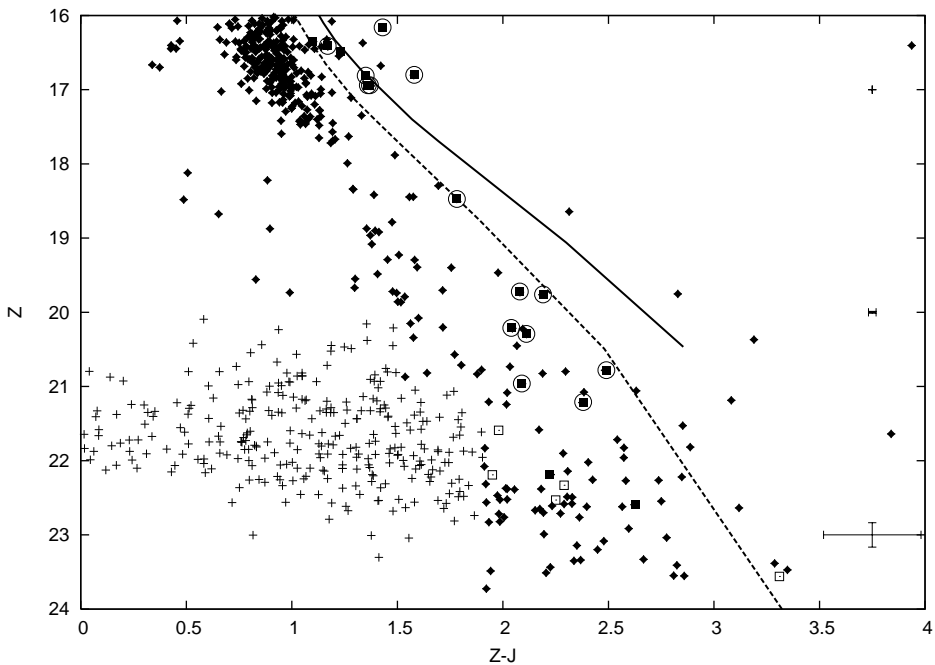


Figure 3. The $Z, Z-J$ CMD for the whole of the survey. The solid line is the NEXTGEN model, and the dotted line the DUSTY model. The crosses are all the objects selected from the $I, I-Z$ (crosses on Figure 2.). The filled diamonds are all objects that met our selection criteria from the $I, I-Z$ and $Z, Z-J$ CMDs. These were selected for proper motion analysis, and were found to be non members. The filled squares are our candidate cluster members (objects that remained after proper motion analysis). The squares are our ZJ only candidates for all four fields that remained after proper motion analysis. The previously identified probable members from Bihain et al. (2006), Moraux et al. (2003) and Bouvier et al. (1998) that remained after our proper motion analysis are identified by open circles around the plotted symbols.

Table 1. 50 and 90% completeness figures for the optical and infrared fields. The positioning of these fields is shown in Figure 1. Note that while WFCAM field 1 corresponds to CFHT fields B, C, R and Q, the individual pawprints, do not correspond on a one to one basis - i.e. field1_00 does not correspond to field B.

Field name	<i>I</i>		<i>Z</i>		WFCAM tile name	WFCAM pawprint name	<i>J</i>	
	50%	90%	50%	90%			50%	90%
B	23.2	22.5	22.3	21.5	field1	00	20.9	19.9
C	23.7	22.6	22.6	21.6	field1	01	20.9	20.1
R	24.0	23.0	22.9	21.6	field1	10	20.9	19.8
Q	23.7	22.5	22.7	21.6	field1	11	20.9	19.7
K	23.6	22.5	23.0	21.9	field2	00	20.9	19.7
L	24.0	22.7	23.0	21.8	field2	01	20.9	19.9
D	23.7	22.4	23.0	21.7	field2	10	21.0	19.9
					field2	11	20.9	19.7
U	23.5	22.5	22.9	21.7	field3	00	19.5	18.8
V	23.8	22.5	22.7	21.7	field3	01	19.0	17.7
T	23.6	22.5	22.6	21.5	field3	10	19.6	18.6
					field3	11	18.9	17.7
I	23.9	22.3	23.1	22.0	field4	00	20.8	19.7
G	23.7	22.7	23.4	22.3	field4	01	20.8	19.7
					field4	10	20.8	19.7
					field4	11	20.8	19.7

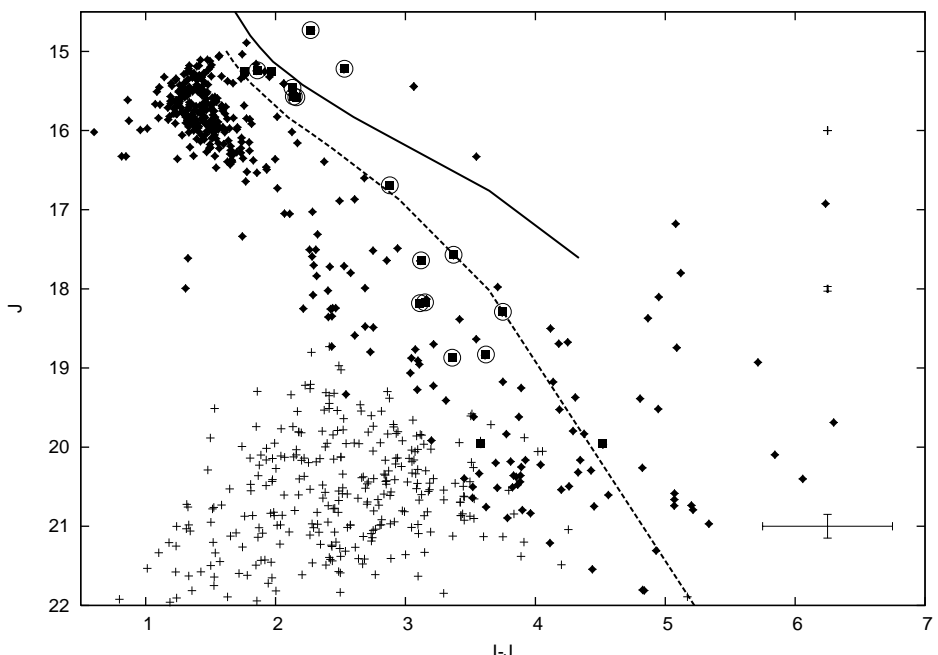


Figure 4. The $J, I-I$ CMD for the whole of the survey. The solid line is the NEXTGEN model, and the dotted line the DUSTY model. The crosses are all the objects selected from the $I, I-Z$ (crosses on Figure 2.). The filled diamonds are all objects that met our selection criteria from the $I, I-Z$ and $Z, Z-J$ CMDs. These were selected for proper motion analysis, and were found to be non members. The filled squares are our candidate cluster members (objects that remained after proper motion analysis). The previously identified members from Bihain et al. (2006), Moraux et al. (2003) and Bouvier et al. (1998) that remained after our proper motion analysis are identified by open circles around the plotted symbols.

ure 2) where the 120 Myr NEXTGEN (Baraffe et al., 1998) and DUSTY (Chabrier et al., 2000) model isochrones (modified to take into account the Pleiades distance of 134 pc e.g. Percival, Salaris & Groenewegen, 2005) served as a guide to the location of the Pleiades sequence. With the uncertainties in both the photometry and the age of the cluster in mind, we selected all objects classed as stellar in both the I and Z data, which in the magnitude range $16.5 < I < 22.5$ lay no more than 0.25 magnitudes to the left of the DUSTY isochrone. All the candidate Pleiads found by Moraux

et al. (2003) and Bihain et al. (2006) lay within ± 0.25 magnitudes of the DUSTY model. Thus our selection criterion is 0.25 magnitudes to the left of the DUSTY model. Below $I=22.5$, the DUSTY model is not red enough to account for known field stars, and so is inappropriate in this effective temperature regime. We have calculated an approximate field star sequence from Tinney, Burgasser & Kirkpatrick (2003) and Hawley et al (2002) and lowered it by 2 magnitudes. This results in the line $I-Z = (I-19.0)/3.5$. This selection is conservative, and is particularly aimed at removing the

bulk of the red tail of the background stars. Subsequently, the initial list of candidates was cross-correlated with our *J* band photometric catalogue (using a matching radius of 2 arcseconds) and a refined photometrically culled sample obtained using the *Z,Z-J* colour-magnitude diagram (Figure 3). These objects are also shown on the *J,I-J* colour-magnitude diagram (Figure 4). As before, the 120 Myr model isochrones were used as a guide to the location of the cluster sequence. With the photometric uncertainties in mind, all candidates with $Z \leq 20$ were retained. All candidates with $20 < Z < 21$ and $Z-J \geq 1.6$ were also retained. Finally, all candidates with $Z > 21$ and $Z-J \geq 1.9$ were retained. These constraints are conservative and are based on the field L and T dwarfs sequence ($Z-J \geq 3$, Chiu et al., 2006) since the DUSTY models are known to be inappropriate in this effective temperature regime. Since our survey is limited by the depth of the *I* band data, all candidates with $Z > 20$ and no *I* band counterpart were also kept.

3.2 Refining the sample using astrometric measurements

To weed out non-members we have measured the proper motion of each candidate brown dwarf, using the *Z* and *J* band data where the epoch difference was 5 years. In this process, only objects lying within 2 arcminutes of each candidate were chosen as potential astrometric reference stars. This compromise provided a sufficiently large number of sources but at the same time minimised the effects of non-linear distortions in the images. Furthermore, objects with large ellipticity (>0.2), classed by the photometric pipeline as non-stellar in the *Z* band data and with $Z < 16$ or $Z > 20$ were rejected. This ensured that, in the main, the astrometric reference sources were not of very low S/N in the *J* band or saturated in the optical data. These criteria generally provided at least 20 suitable stars per candidate brown dwarf.

Six coefficient transforms between the epoch 1 *Z* band images and the epoch 2 *J* band images were calculated using routines drawn from the STARLINK SLALIB package. The iterative fitting rejects objects having residuals greater than 3σ , where σ is robustly calculated as the median of absolute deviation of the reference star residuals, scaled by the appropriate factor (1.48) to yield an equivalent RMS. Once the routine had converged the relative proper motions in pixels were calculated by dividing the fitting residuals of each candidate by the epoch difference. For our data the epoch difference is approximately 5 years. Subsequently, the astrometric motion in milliarcseconds per year in RA and DEC was derived by folding these values through the World Coordinate System transform matrix of the relevant WFCAM image.

To estimate the errors on our proper motions measurements, we have injected fake stars into both the *Z* and *J* band data, in a similar fashion to that described in section 2.3. However, here we have determined the difference between the inserted position and the photometric pipeline estimate of the centroid of each star. Assuming that the differences between these two locations are normally distributed, we have divided the fake stars into 3 magnitude bins in each photometric band ($Z \leq 21$, $23 \geq Z > 21$, $24 \geq Z > 23$, $21 \geq J > 17$) and fit 2d Gaussians to estimate the 1-sigma centroiding uncertainty as a function of source brightness.

We find that in the *Z* band data, for objects with magnitudes $Z \leq 21$, the centroiding uncertainty is equivalent to 3 mas yr^{-1} in each axis, while for objects with $23 \geq Z > 21$ this number increases to 8 mas yr^{-1} . For our faintest *Z* band objects, $24 \geq Z > 23$, the centroiding uncertainty is equivalent to 12 mas yr^{-1} in each axis. In the *J* band data, for objects with magnitudes $21 \geq J > 17$, the centroiding uncertainty is equivalent to 5 mas yr^{-1} in each axis. Thus

for our brightest candidates ($Z < 21$, $J < 19$), the quadratic sum of the *Z* and *J* band centroiding errors is less than or comparable to the RMS of the residuals of the linear transform fit, which is typically $5\text{--}10 \text{ mas yr}^{-1}$ in each axis. We adopt this latter quantity as the proper motion uncertainty in both the RA and DEC directions for these objects. It is worth noting at this point that both the stars and brown dwarfs of the Pleiades appear to be in a state of dynamical relation (e.g. Pinfield et al. 1998, Jameson et al. 2002), where the velocity dispersion of the members is proportional to $1/M^{0.5}$, where M is mass. Based on an extrapolation of the data in Figure 4 of Pinfield et al. (1998), we would expect our lowest mass brown dwarf members ($0.01\text{--}0.02M_{\odot}$) to have velocity dispersion of $\sim 7 \text{ mas yr}^{-1}$. This velocity dispersion should be added quadratically to the above uncertainties. Our final adopted proper motion selection, effectively a radius of 14 mas yr^{-1} , is described below, and the velocity dispersion is small compared to this.

We fitted the proper motions of all of our photometric candidates (excluding the *ZJ* only candidates) with a 2D Gaussian, which centred around $1.1, -7 \text{ mas yr}^{-1}$. This Gaussian had a σ of 14.0 . We were not able to fit two Gaussians, one to the background stars and one to the Pleiades dwarfs, as described in Moraux et al. (2003), since only ≈ 30 objects have the correct proper motion for cluster membership. Consequently, we only selected objects to be proper motion members if they had proper motions that fell within 1σ of the proper motion of the cluster at $+20.0, -40.0 \text{ mas yr}^{-1}$ (Jones 1981; Hambly, Jameson & Hawkins, 1991; Moraux et al., 2001). We required the selection criteria to be 1σ , as extending this to 2σ , would seriously overlap with the field stars centred on $0,0$. We did however extend the selection criteria to 1.5σ , which yielded 14 additional objects, however all were rejected due to their bright, but blue ($J \approx 17.0$, $I-Z < 1.0$) positions on the *I,I-Z* CMD, which led us to believe that they were field objects. We also attempted to tighten our selection criteria to a circle with radius 10 mas yr^{-1} . This selection meant that we lost as possible members objects PLZJ 78, 9, 77, 23 (see Table 4). PLZ 79, 9 and 77 have all been identified and confirmed as proper motion members by Bihain et al. (2006), Moraux et al. (2001), and Bouvier et al. (1998). Unfortunately, as we cannot fit two Gaussians to our data, we cannot calculate a probability of membership for these objects by the standard method as defined by Sanders (1971). The proper motion measurements may be found in Table 4, as well as the *I, Z, J, H* and *K* magnitudes for these candidate members to the cluster.

We have attempted to use control data to determine the level of contamination within our data, however, the numbers involved are very small, so any calculated probability will be rather uncertain. We used as controls, two circles of radius 14.0 mas yr^{-1} , at the same distance from $0,0$ proper motion as the Pleiades. We then separated the data into one magnitude bins, and calculated the probability for each magnitude bin, using equation 1.

$$P_{\text{membership}} = \frac{N_{\text{cluster}} - N_{\text{control}}}{N_{\text{cluster}}} \quad (1)$$

Where $P_{\text{membership}}$ is the probability of membership for that magnitude bin, N_{cluster} is the number of stars and contaminants within the cluster circle in that magnitude bin. N_{control} is the number of dwarfs in the control circle of proper motion space, see Figure 4. $N_{\text{cluster}} - N_{\text{control}}$ is the number of Pleiads. It can be seen that the probability depends on where the control circle is located. Thus as well as using control circles, we use an annulus and scale down the count to an area equal to that of a control circle. Note that Figure 5 is for all of the magnitude bins together. Figure 6 is the same as Figure 5, but for the *ZJ* selected objects only. The statistics are

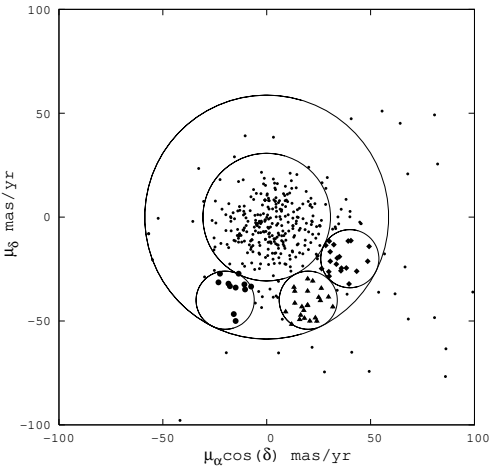


Figure 5. Proper motion vector diagram of the photometrically selected candidate members. The filled triangles are candidate and known cluster members. The filled diamonds and filled circles are the two separate control clusters used. The annulus used for the radial method is also plotted.

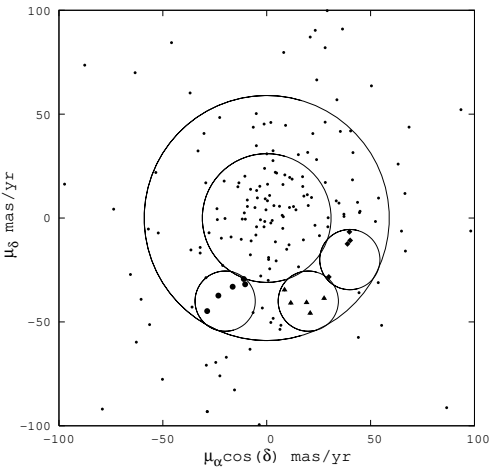


Figure 6. Proper motion vector diagram of the photometrically selected candidate members. The filled triangles are candidate cluster members selected from the $Z, Z-J$ CMD only. The filled diamonds and filled circles are the two separate control clusters used. The annulus used for the radial method is also plotted.

much poorer for the individual magnitude bins and the probabilities are correspondingly more uncertain. It can be seen in Figure 4 that there is not a symmetrical distribution of proper motions. In fact the distribution in the Vector point diagram, is a classical "velocity ellipsoid" displaced from zero by reflex motion from the Sun's peculiar velocity, and happens to be in the direction of the Pleiades proper motion vector. We have therefore probably underestimated the contamination, as the annulus method of calculating probabilities assumes that the vector point diagram has a circularly symmetric distribution of objects. These probabilities are shown in Table 2, and probabilities derived in the same way but for the ZJ only candidates can be found in Table 3.

An alternative approach to estimating the contamination is the use the field *L* and *T* dwarf luminosity functions. Chabrier (2005) gives the *T* dwarf luminosity function as being 10^{-3}

dwarfs/ $\text{pc}^3/\text{unit } J \text{ mag interval}$. Our 7 *L* and *T* dwarf candidates cover a total of 0.7 mag in the *J* band. Note PLZJ 323 and 23 may be late *L* dwarfs but we include them in this analysis. The volume of space we use is 836 pc^3 , based on 2.5 square degrees and a distance to the Pleiades of $134 \pm 30 \text{ pc}$ (Percival et al., 2005). This distance range corresponds to a distance modulus range of ± 0.5 magnitudes, which is generous, given that the sequence shown in figure 8 is clearly narrower than ± 0.5 magnitudes. Thus the expected number of contaminating field dwarfs is 0.6. In addition to this, field *T* dwarfs are unlikely to have the same proper motion as the Pleiades, thus reducing the 0.6 further. For the field *L* dwarfs with $M_J \approx 13.0$ (i.e. $J \approx 18.5$ at the distance of the Pleiades) the luminosity function is 3×10^{-4} dwarfs/ $\text{pc}^3/\text{unit } J \text{ mag interval}$ (Chabrier, 2005). A similar calculation then gives 0.25 contaminating *L* dwarfs which should be further reduced by considering proper motions. It is thus clear that the field luminosity function indicates that contamination by field *L* and *T* dwarfs should be negligible.

4 RESULTS

Most of these objects, except two bright objects and the faintest seven have been documented before in surveys - Moraux et al (2003) and Bihain et al (2006). We recovered all of these objects within our overlapping area, and none were rejected by our IZ photometric selection. The objects we recovered were BRB 4, 8, 17, 13, 19, 21, 22, 27 and 28 and PLIZ 2, 3, 5, 6, 13, 14, 19, 20, 26, 28, 31, 34, 35 and 36. PLIZ 18, 27 and 39 were found to have no *J* counterpart in our catalogues. Of these objects, BRB 19 and PLIZ 14 and 26 met by our selection criteria on the $Z, Z-J$ CMD, however they were too blue in their $Z-J$ colour for their place on the sequence. Out of the remaining objects we find that we agree with the proper motion measurements as calculated by Bihain et al.(2006) for PLIZ 28, which we believe is a member of the cluster. We agree with Bihain et al.(2006) over their candidates BRB 13 and BRB 19 that they are not proper motion members to the cluster, however we disagree with their proper motion measurement for BRB 19. We also find that PLIZ 5 is a non member to the cluster - ie its proper motion measurement is not within 14 mas yr^{-1} of the cluster proper motion value. We find that PLIZ 14 and 26 are not proper motion members to the cluster, as well as not having met our selection criteria. PLIZ 26 was found to have a proper motion measurement of $35.73 \pm 9.00, -25.83 \pm 6.96$, which did not fall within 14 mas yr^{-1} of the cluster, and also missed the selection made with the wider circle (21 mas yr^{-1}) as well. We find that PLIZ 19, 20, 34 and 36 are not proper motion members to the cluster. However this means we disagree with Moraux et al. (2003), over their object PLIZ 20. They find a proper motion of $25.6 \pm 7.3, -44.7 \pm 7.4 \text{ mas yr}^{-1}$ for it. Our proper motion measurement is $0.88 \pm 15.86, -0.92 \pm 8.42 \text{ mas yr}^{-1}$. It is possible that this object has been adversely affected by its position on the edge of one of the WFCAM chips, thus reducing the number of reference stars used to calculate its proper motion. An alternative method of measuring the proper motion using all the objects on the same chip produced a measurement of $19.14 \pm 11.06, -28.989 \pm 11.94 \text{ mas yr}^{-1}$. This value does meet our selection criteria, and has been previously accepted as a member. We suggest PLIZ 20 is likely to be a member because of this.

We find that PLIZ 2, 3, 6, 31 and 35 are all proper motion members to the cluster. In addition to this, we find 2 brighter new candidate members to the cluster. These objects are bright enough to have appeared in previous surveys, and in the UKIDSS Galactic cluster survey (GCS). We also have 2 fainter new members to the

Table 4. Name, coordinates, Z , I , J , H and K magnitudes for our members to the cluster. The errors quoted are internal (from photon counting). The systematic calibration errors are 2% in the J , H and K wavebands (Warren *et al.*, 2007), and 3% in the I and Z wavebands. The J , H and K magnitudes are on the MKO system. Previously discovered members also have their other known names listed from Moraux *et al.* (2003), Bihain *et al.* (2006) and Bouvier *et al.* (1998). The H and K band magnitudes are taken from the UKIDSS Galactic Cluster Survey with the exceptions of PLZJ 23, 93, 721 and 235 which have their H band magnitudes listed from our H survey. The K band magnitude for PLZJ 93 is from our UFTI photometry, and PLZJ 23 is from LIRIS service time. The final 5 objects in the table are our candidates selected from the ZJ data only.

Name	Alternate name	RA	dec	$\mu_\alpha \cos\delta$	μ_δ	I	Z	J	H	K
		J2000.0		mas yr $^{-1}$						
PLZJ 29	BRB4	03 44 23.23	+25 38 45.11	23.40 \pm 8.24	-48.51 \pm 6.34	17.005 \pm 0.001	16.163 \pm 0.001	14.732 \pm 0.001	14.132 \pm 0.004	13.744 \pm 0.004
PLZJ 56		03 44 53.51	+25 36 19.46	19.68 \pm 7.34	-35.63 \pm 5.29	17.012 \pm 0.001	16.351 \pm 0.001	15.250 \pm 0.001	14.650 \pm 0.005	14.342 \pm 0.006
PLZJ 45	BRB8, CFHT-PL-7	03 52 58.2	+24 17 31.57	19.72 \pm 4.95	-42.37 \pm 7.44	17.101 \pm 0.001	16.417 \pm 0.001	15.247 \pm 0.001	14.614 \pm 0.005	14.251 \pm 0.006
PLZJ 50		03 43 55.98	+25 36 25.45	13.48 \pm 8.24	-35.65 \pm 5.38	17.239 \pm 0.001	16.496 \pm 0.001	15.268 \pm 0.001	14.693 \pm 0.006	14.319 \pm 0.006
PLZJ 60	CFHT-PL-10	03 44 32.32	+25 25 18.06	16.93 \pm 7.76	-43.15 \pm 5.72	17.592 \pm 0.001	16.810 \pm 0.001	15.460 \pm 0.001	14.884 \pm 0.007	14.465 \pm 0.006
PLZJ 78	PLIZ2	03 55 23.07	+24 49 05.18	19.72 \pm 10.45	-29.74 \pm 10.45	17.719 \pm 0.001	16.948 \pm 0.001	15.574 \pm 0.001	14.963 \pm 0.007	14.552 \pm 0.007
PLZJ 46	PLIZ3, BRB11	03 52 67.20	+24 16 01.00	19.55 \pm 5.15	-42.58 \pm 7.57	17.742 \pm 0.001	16.945 \pm 0.001	15.583 \pm 0.001	14.966 \pm 0.007	14.503 \pm 0.008
PLZJ 9	PLIZ6, BRB9	03 53 55.09	+23 23 36.38	24.13 \pm 13.83	-50.10 \pm 22.71	17.752 \pm 0.001	16.804 \pm 0.001	15.222 \pm 0.001	14.548 \pm 0.005	14.054 \pm 0.005
PLZJ 11	PLIZ20	03 54 05.33	+23 33 59.71	9.14 \pm 11.06	-28.98 \pm 11.94	19.571 \pm 0.004	18.563 \pm 0.004	16.691 \pm 0.005	15.980 \pm 0.016	15.436 \pm 0.016
PLZJ 77	PLIZ28, BRB18	03 54 10.04	+23 17 52.28	12.01 \pm 14.59	-51.60 \pm 15.84	20.760 \pm 0.010	19.728 \pm 0.010	17.647 \pm 0.010	16.789 \pm 0.031	16.131 \pm 0.030
PLZJ 21	PLIZ31	03 51 47.65	+24 39 59.18	17.84 \pm 9.41	-44.92 \pm 8.03	20.944 \pm 0.014	19.762 \pm 0.013	17.575 \pm 0.012	16.774 \pm 0.026	16.089 \pm 0.028
PLZJ 10	PLIZ35, BRB15	03 52 31.19	+24 46 29.61	15.84 \pm 8.88	-49.34 \pm 6.24	21.293 \pm 0.018	20.292 \pm 0.016	18.181 \pm 0.022	17.118 \pm 0.041	16.506 \pm 0.0416
PLZJ 4	BRB21	03 54 10.25	+23 41 40.67	29.74 \pm 13.17	-38.46 \pm 8.88	21.322 \pm 0.010	20.215 \pm 0.013	18.171 \pm 0.010	17.141 \pm 0.045	16.377 \pm 0.039
PLZJ 61	BRB22	03 44 31.27	+25 35 14.97	25.82 \pm 7.89	-40.21 \pm 8.47	22.043 \pm 0.030	20.782 \pm 0.026	18.298 \pm 0.020	17.393 \pm 0.059	16.657 \pm 0.04
PLZJ 32	BRB27	03 44 27.27	+25 44 41.99	25.03 \pm 11.52	-38.65 \pm 23.46	22.235 \pm 0.040	20.962 \pm 0.029	18.871 \pm 0.030	17.793 \pm 0.094	16.950 \pm 0.070
PLZJ 37	BRB28	03 52 54.92	+24 37 18.85	18.13 \pm 11.53	-48.68 \pm 11.38	22.452 \pm 0.05	21.216 \pm 0.041	18.839 \pm 0.030	17.742 \pm 0.071	16.921 \pm 0.058
PLZJ 23		03 51 53.38	+24 38 12.11	20.75 \pm 10.51	-50.05 \pm 9.96	23.541 \pm 0.140	22.187 \pm 0.112	19.960 \pm 0.100	19.362 \pm 0.100	18.510 \pm 0.030
PLZJ 93		03 55 13.00	+24 36 15.8	13.11 \pm 14.36	-33.77 \pm 12.97	24.488 \pm 0.370	22.592 \pm 0.164	19.968 \pm 0.080	19.955 \pm 0.100	19.420 \pm 0.100
PLZJ 323		03 43 55.27	+25 43 26.2	29.87 \pm 12.05	-39.37 \pm 11.70	-	21.597 \pm 0.054	19.613 \pm 0.076	-	-
PLZJ 721		03 55 07.14	+24 57 22.34	19.18 \pm 22.23	-40.70 \pm 12.38	-	22.195 \pm 0.092	20.248 \pm 0.116	20.417 \pm 0.123	-
PLZJ 235		03 52 32.57	+24 44 36.64	20.92 \pm 12.16	-45.84 \pm 11.75	-	22.339 \pm 0.115	20.039 \pm 0.112	20.245 \pm 0.127	-
PLZJ 112		03 53 19.37	+24 53 31.85	8.56 \pm 14.08	-34.59 \pm 19.99	-	22.532 \pm 0.116	20.281 \pm 0.143	-	-
PLZJ 100		03 47 19.19	+25 50 53.3	20.23 \pm 14.27	-37.28 \pm 23.82	-	23.563 \pm 0.373	20.254 \pm 0.114	-	-

Table 2. Probability of membership, magnitude range for our methods of calculating probabilities of membership using the annulus as well as the two control areas.

Probability annulus	Probability $\mu_\alpha \cos\delta = -20 \text{ mas yr}^{-1} \mu_\delta = -40 \text{ mas yr}^{-1}$	Probability $\mu_\alpha \cos\delta = +40 \text{ mas yr}^{-1} \mu_\delta = -20 \text{ mas yr}^{-1}$	Magnitude range Z
0.67	0.25	0.0	16 - 17
0.82	0.66	0.0	17 - 18
0.88	1.00	0.0	18 - 19
0.84	1.00	0.0	19 - 20
1.00	1.00	1.00	20 - 21
0.88	0.50	1.00	21 - 22
0.61	1.00	0.00	22 - 23

Table 3. Probability of membership, magnitude range for our methods of calculating probabilities of membership using the annulus as well as the two control areas for our candidates selected from the ZJ data only.

Probability annulus	Probability $\mu_\alpha \cos\delta = -20 \text{ mas yr}^{-1} \mu_\delta = -40 \text{ mas yr}^{-1}$	Probability $\mu_\alpha \cos\delta = +40 \text{ mas yr}^{-1} \mu_\delta = -20 \text{ mas yr}^{-1}$	Magnitude range Z
0.61	1.00	1.00	21 - 22
0.35	0.67	0.33	22 - 23
-0.16	-2.00	0.00	23 - 24

cluster, and 5 objects selected using the ZJ photometry only. All of the objects identified as cluster members in this work are presented in Table 4. Two WFCAM tiles, 1 and 4, (see Figure 1) also had deep H band photometry. These tiles were observed at the same time as the J band imaging, and were observed under the same conditions, but with the exception that microstepping was not used. These data were reduced using the same pipeline as the J band data, but the photometry and object detection used a core radius of 2.5 pixels in this case. Fortunately these tiles also covered our faintest, previously undiscovered Pleiades candidates, PLZJ 23 and PLZJ 93, as well as two of the candidates selected from the ZJ data only, PLZJ 721 and 235.

The UKIDSS Galactic Cluster survey (GCS) has also covered the entire area at J , H and K . The UKIDSS data are reduced using the same pipeline as the WFCAM data (see Dye et al, 2006 for details of the pipeline).

We also have used UKIRT service time to measure photometry for PLZJ 93 in the K band. This observation was taken on 09/09/2006 in seeing of better than $1.1''$ using the UKIRT Fast Track Imager (UFTI), with a five point dither pattern. The data were reduced using the ORAC-DR pipeline, and the photometry was calibrated using UKIRT Faint Standard 115.

The K band photometry for PLZJ 23 was obtained on the night of 05/03/2007 using the long slit intermediate resolution spectrograph (LIRIS) on the William Hershel Telescope in service time, using a nine point dither pattern in seeing of $\approx 0.9''$. The data were reduced using IRAF and astrometrically and photometrically calibrated using 2MASS. The colour transforms presented in Carpenter, (2001) were used to calculate the K band magnitude from the K_S magnitude.

Thus we have I , Z , J , H and K band photometry for the majority of our Pleiades candidates. However H or K band photometry is still needed for PLZJ 323, 721, 235, 112 and 100, (see Table 4). Figures 7 and 8 show the K , $J-K$ and H , $J-H$, colour magnitude diagrams, together with the NEXTGEN (Baraffe et al, 1998) and DUSTY (Chabrier et al, 2000) models for the Pleiades age of 120 Myrs (Stauffer et al 1998). The candidate members listed in Table

4 are also plotted in Figures 3 and 4 for clarity. In both of these diagrams the M dwarf tail, the redward L dwarf sequence and the L to T blueward transition sequence are clear. The L-T transition sequence of course only has two objects plotted on it on Figure 7 as we have no K band photometry for the ZJ candidates. As expected the K , $J-K$ diagram gives the best differentiation between the sequences. The redward L sequence in this diagram agrees with that found by Lodieu et al,(2007b) derived from a much greater area of the Pleiades by the UKIDSS GCS. The GCS is not sensitive enough to see the L-T blueward transition sequence however. The K , $J-K$ diagram also shows the separation between single and binary dwarfs quite clearly. Note that the DUSTY theoretical track is too flat compared to our empirical sequence, see figures 7 and 8.

PLZJ 23, 93, 721 and 235 have $J-H$ colours of 0.60, 0.00, -0.17 and -0.21 respectively. Comparing these colours with the spectral type colour relations of field dwarfs described in Leggett et al. (2002), yields estimated spectral types of T1.5, T4.5, T6 and T6 respectively. PLZJ 93 has $J-K=0.60$ which gives a spectral type of T3 (Leggett et al., 2002), which is consistent with the spectral type derived from the $J-H$ colour (T4.5), within the errors. We also can calculate a $H-K$ colour for this dwarf of 0.6, however the $H-K$ colour is not a good choice for spectral typing, for instance, $H-K=0.6$ covers a range of spectral types from L1 to T3 (Chiu et al., 2006). The $Z-J$ colour is also not a good choice of colour for measuring spectral types until the later T dwarfs ($>T2$)(Hawley et al., 2002). PLZJ 23 has $J-K=1.45$, which gives a spectral type of between L8 and T1. The $H-K$ colour for this dwarf is 0.85. We may thus assume that PLZJ 23 has a spectral type between L8 and T1.5, and likewise that PLZJ 93 has a spectral type of between T3 and T5 to take into account the photometric errors. It should be noted that the Z band quoted in Hawley et al., (2002) is for the Sloan filter system, and so for this reason we have not chosen to use it to spectral type our objects. We believe that the $J-H$ colour gives the best estimate available to us of spectral types. Two of the three candidate members without H band photometry PLZJ 112 and 100 have fainter J magnitudes than PLZJ 23 and 93, and so it is likely that they are also T dwarfs. PLZJ 323 is brighter and is therefore

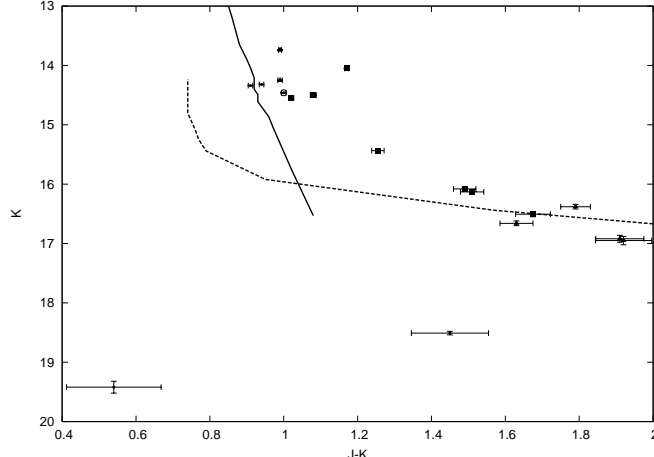
Table 4.

Figure 7. The $K, J-K$ CMD for our candidate cluster members. The solid line is the NEXTGEN model of Baraffe et al. (1998), and the dotted line is the DUSTY model of Chabrier et al. (2000). The filled squares are the candidates identified by Moraux et al. (2003), the filled triangles are the candidates identified by Bihain et al. (2006), the object enclosed by the open circle is CFHT-PL-10 identified by Bouvier et al. (1998). The objects marked by small points are our new candidate members. One of our T dwarf candidates, PLZJ 93, is found to the bottom of the plot, with a $J-K$ of ≈ 0.6 . PLZJ 23 is also present with a $J-K$ of 1.45.

probably a late L dwarf. Indeed our faintest candidate at Z , PLZJ 100, may be a very late T dwarf, however this assumption is made using its $Z-J$ colour, which is very red. Using J magnitudes and the COND models of Baraffe et al. (2003) for 120 Myrs (the DUSTY models are no longer appropriate for calculating masses for objects this faint in the Pleiades), we calculate masses of $\approx 11 M_{Jup}$ for PLZJ 23, 93, 323, 721, 235, 112 and 100. More photometry in the H and K bands is clearly needed to improve and extend these estimates of the spectral types.

5 MASS SPECTRUM

To calculate the mass spectrum, we first divided the sample into single dwarfs or single dwarfs with possible low mass companions and dwarfs that are close to 0.75 magnitudes above the single star sequence in the $K, J-K$ colour magnitude diagram. The latter we assume to be equal mass binaries and count them as dwarfs with masses the same as a dwarf on the single dwarf sequence below them. From Figures 3, 4, 7 and 8 it can be seen that there are 2 such binaries all with $J-K \approx 1$. Dwarfs with $J-K < 1.2$ are assigned masses using their H magnitudes and the NEXTGEN models (Baraffe et al. 1998). For $1.2 < J-K < 2.0$ we use the DUSTY models (Chabrier et al., 2000) and the $J-H$ colour to assign a mass. Finally the T dwarf masses were calculated from their J magnitudes and the COND models (Baraffe et al., 2003). The masses were binned into three mass intervals, covering the low, medium and high mass ranges and the numbers per bin are weighted by the probabilities of membership calculated using the annulus, and the bin width has been taken into account. The candidate members with negative probabilities are obviously omitted from the mass spectrum. The resultant mass spectrum is shown in Figure 9. The

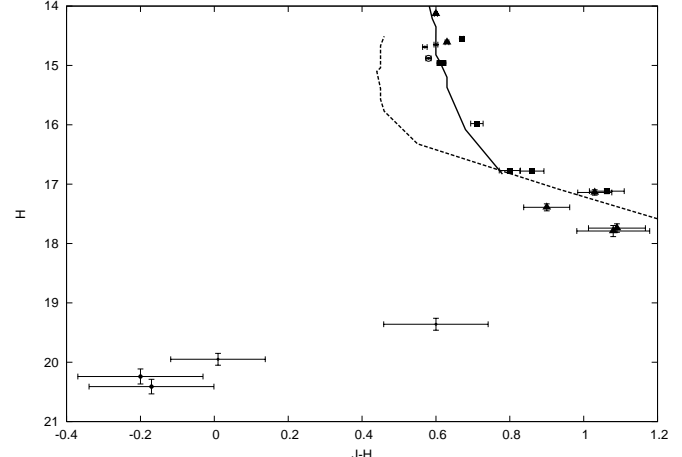


Figure 8. The $H, J-H$ CMD for our candidate cluster members. The filled squares are the candidates identified by Moraux et al. (2003), the filled triangles are the candidates identified by Bihain et al. (2006), the object enclosed by the open circle is CFHT-PL-10 identified by Bouvier et al. (1998). The objects marked by small points are our new candidate members. The filled diamonds are the two candidates with H magnitudes selected from the ZJ data only. The solid line is the NEXTGEN model of Baraffe et al (1998), and the dotted line is the DUSTY model of Chabrier et al. (2000).

errors are poissonian. Clearly the statistics are very poor, due to the small number of objects being dealt with. Using linear regression we have fitted our data to the relationship $dN/dM \propto M^{-\alpha}$, and calculate $\alpha = 0.35 \pm 0.31$. This is lower but still in agreement with values presented in the literature (within 1σ), however the error on this value is large, and the statistics are poor due to the small numbers involved. If we take into account the fact that the last mass bin is only 50% complete (using Tables 1 and 4), then the lowest mass bin can be increased by 50% to compensate. If we then fit these data, we derive a value for α of 0.62 ± 0.14 , which is in agreement with the literature. Alternatively, we can discount this final low mass bin as being incomplete and simply omit it from the fit. In this case we calculate a value for α of 0.86. We have only displayed the mass spectrum for the cluster in the area and magnitude surveyed. This is to avoid trying to take into account biases caused by some areas being more studied than others, and also because we are only adding a maximum of 9 objects to the mass spectrum, 7 of which have low probabilities of membership and small masses, and so are not likely to affect previous results a large amount. The mass spectrum appears to be rising towards the lowest masses, but this is not statistically significant due to the large error bars.

6 CONCLUSIONS

We have confirmed a number of L dwarf candidates in the Pleiades. However the main result in this paper is the discovery of seven L and T dwarf Pleiads of masses $\approx 11 M_{Jup}$, below the $13 M_{Jup}$ deuterium burning limit that is often used, somewhat artificially as the upper bound for planetary masses. Further H and K band photometry, currently lacking for some of these candidates, will improve confidence in their membership of the cluster. Planetary mass brown dwarfs have, of course, been claimed in the Orion nebula

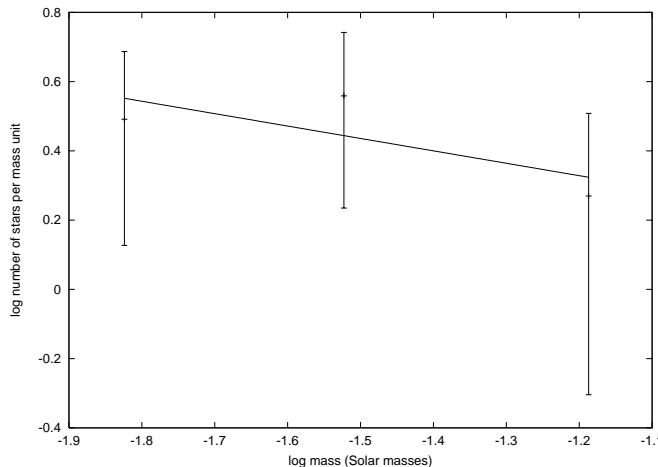


Figure 9. The mass spectrum for our Pleiades candidate members. The mass bin is in units of M_{\odot} . The solid line is the fit to the data, ($\alpha=0.35\pm0.31$).

(Lucas & Roche 2000) and in the σ -Ori cluster (Zapatero-Osorio et al., 2002). These clusters both have very young ages and may also have a spread of ages (Béjar et al., 2001), making mass determinations somewhat uncertain. Lodieu et al. (2006, 2007a) have also found planetary mass brown dwarfs in the Upper Scorpius Association which has an age of 5 Myrs (Preibisch & Zinnecker, 2002). At very young ages the theoretical models may have significant errors when used to assign masses (Baraffe et al., 2002). Our result is the first detection of planetary mass objects in a mature cluster whose age is well established. It strengthens the case that the star formation process can produce very low mass objects.

7 ACKNOWLEDGEMENTS

SLC, NL, and PDD acknowledge funding from PPARC. We also acknowledge the Canadian Astronomy Data Centre, which is operated by the Dominion Astrophysical Observatory for the National Research Council of Canada's Herzberg Institute of Astrophysics. This work has been based on observations obtained at the Canada-France-Hawaii Telescope (CFHT) which is operated by the National Research Council of Canada, the Institut National des Sciences de l'Univers of the Centre National de la Recherche Scientifique of France, and the University of Hawaii. Observations were also made at the United Kingdom Infrared Telescope, which is operated by the Joint Astronomy Centre on behalf of the U.K. Particle Physics and Astronomy Research Council. This publication makes use of data products from the Two Micron All Sky Survey, which is a joint project of the University of Massachusetts and the Infrared Processing and Analysis Center/California Institute of Technology, funded by the National Aeronautics and Space Administration and the National Science Foundation. This research has made use of NASA's Astrophysics Data System Bibliographic Services, the WHT service programme, and the UKIRT service programme. We would like to thank the referee V.J.S. Béjar for his comments which have improved the paper.

REFERENCES

Adams F. C., Fatuzzo M., 1996, ApJ, 464, 256

Baraffe I., Chabrier G., Allard F., Hauschildt P. H., 1998, A&A, 332, 403

Baraffe I., Chabrier G., Allard F., Hauschildt P. H., 2002, A&A, 382, 563

Baraffe I., Chabrier G., Barman T. S., Allard F., Hauschildt P. H., 2003, A&A, 402, 701

Bate M. R., 2004, Ap&SS, 292, 297

Béjar V. J. S. et al., 2001, ApJ, 556, 830

Bihain G., Rebolo R., Béjar V. J. S., Caballero J. A., Bailer-Jones C. A. L., Mundt R., Acosta-Pulido J. A., Manchado Torres A., 2006, A&A, 458, 805

Boss A. P., 2001, ApJ, 551, L167

Bouvier J., Stauffer J. R., Martín E. L., Barrado y Navascués D., Wallace B., Béjar V. J. S., 1981, A&A, 336, 490

Burgasser A. J., Kirkpatrick J. D., McGovern M. R., McLean I. S., Prato L., Reid I. N., 2004, ApJ, 604, 827

Carpenter J. M., 2001, AJ, 121, 2851

Chabrier G., Baraffe I., Allard F., Hauschildt P. H., 2000, ApJ, 542, 464

Chabrier G., 2005, in Corbelli E., Palla F., Zinnecker H., eds, ASSL vol. 327: The Initial Mass function 50 Years Later

Chiu K., Fan X., Leggett S. K., Goliowski D. A., Zheng W., Geballe T. R., Schneider D. P., Brinkmann J., 2006, AJ, 131, 2722

Close L. M., et al., 2005, Nature, 433, 286

Dobbie P. D., Kenyon F., Jameson R. F., Hodgkin S. T., Pinfield D. J., Osborne S. L., 2002, MNRAS 335 687

Dye S., et al., 2006, MNRAS, 372, 1227

Goodwin S. P., Whitworth A. P., Ward-Thompson D., 2004, A&A, 414, 633

Hambly N. C., Jameson R. F., Hawkins M. R. S., 1991, MNRAS, 253, 1

Hawley S. L., et al., 2002, AJ, 123, 3049

Hillenbrand L. A., White R. J., 2004, ApJ, 604, 741

Hodgkin S. T., et al., 2007, in preparation

Irwin M. J., 1985, MNRAS, 214, 575

Irwin M. J., Lewis J., 2001, NewAR, 45, 105

Irwin M. J., et al., in preparation

Jameson R. F., Dobbie P. D., Hodgkin S. T., Pinfield D. J., 2002, MNRAS, 335, 853

Janson M., Brandner W., Lenzen R., Close L., Nielsen E., Hartung M., Hening T., Bouy H., in press A&A,

Jones B. F., 1981, AJ, 86, 290

Landolt A. U., et al., 1992, AJ, 104, 340

Leggett S. K., et al., 2002, ApJ, 564, 452

Lodieu N., Hambly N. C., Jameson R. F., 2006, MNRAS, 373, 95

Lodieu N., Hambly N. C., Jameson R. F., Hodgkin S. T., Carraro G., Kendall T. R., 2007a, MNRAS, 374, 372

Lodieu N., et al. 2007b, in preparation

Low C., Lynden-Bell D., 1976, MNRAS, 176, 367

Lucas P. W., Roche P. F., 2000, MNRAS, 314, 654

Luhman K. L., Stauffer J. R., Mamajek E. E., 2005, ApJ, 628, 69L

Moraux E., Bouvier J., Stauffer J. R., 2001, A&A, 367, 211

Moraux E., Bouvier J., Stauffer J. R., Cullindre J-C., 2003, A&A, 400, 891

Muench A. A., Lada E. A., Lada C. J., Alves J., 2002, ApJ, 573, 366

Muench A. A., et al., 2003, AJ, 125, 2029

Padoan P., Nordlund Å., 2002, ApJ, 576, 870

Percival S. M., Salaris M., Groenewegen M. A. T., 2005, A&A, 429, 887

Pinfield D. J., Jameson R. F., Hodgkin S. T., 1998, MNRAS, 299, 955

Pinfield D. J., Hodgkin S. T., Jameson R. F., Cossburn M. R., Hambly N. C., Devereux N., 2000, MNRAS, 313, 347

Preibisch T., Zinnecker H., 2002, AJ, 123, 1613

Sanders W. L., 1971 A&A, 14, 226

Stassun K. G., Mathieu R. D., Valenti J. A., 2006, Nature, 440, 311

Stauffer J. R., Schultz G., Kirkpatrick J. D., 1998, ApJ, 499, 199L

Tinney C. G., Burgasser A. J., Kirkpatrick J. D., 2003, AJ, 126, 975

Warren S. J., et al., 2007, MNRAS, 375, 213

Whitworth A. P., Goodwin S. P., 2005, AN, 326, 899

Zapatero Osorio M. R., Rebolo R., Martín E. L., Basri G., Magazzú A., Hodgkin S. T., Cossburn M. R., Jameson R. F., 1998, in Donahue, R. A., Bookbinder J. A., eds, ASP Conf. Ser. Vol. 154, Cool Stars, Stellar Systems, and the Sun, p.1912

Zapatero Osorio M. R., Béjar V. J. S., Martín E. L., Rebolo R., Barrado y Navascués D., Mundt R., Eislöffel J., Caballero J. A., 2002, ApJ, 578, 536

Zapatero Osorio M. R., Lane B. F., Pavlenko Y., Martín E. L., Britton M., Kulkarni S. R., 2004, ApJ, 615, 2004

Errata: Proper motion candidate members of the Pleiades

S. L. Casewell¹*, P. D. Dobbie^{1,2}, S. T. Hodgkin³, E. Moraux⁴, R. F. Jameson¹,
N. C. Hambly⁵, J. Irwin³ and N. Lodieu^{6,1}

¹*Department of Physics and Astronomy, University of Leicester, University Road, Leicester LE1 7RH, UK*

²*Anglo-Australian Observatory, PO Box 296, Epping NSW 1710 Australia*

³*CASU, Institute of Astronomy, University of Cambridge, Madingley Road, Cambridge, CB3 0HA, UK*

⁴*Laboratoire d’Astrophysique, Observatoire de Grenoble, Université Joseph Fourier, BP 53, 38041 Grenoble Cedex 9, France*

⁵*Scottish Universities Physics Alliance (SUPA), Institute for Astronomy, School of Physics, University of Edinburgh,*

Royal Observatory, Blackford Hill, Edinburgh EH9 3HJ

⁶*Instituto de Astrofísica de Canarias, Vía Láctea s/n, E-38205 La Laguna, Tenerife, Spain*

3 December 2018

The paper ‘‘Proper motion L and T dwarf candidate members of the Pleiades’’ was published in the *Monthly Notices of the Royal Astronomical Society*, 2007, 378, 1131. It has come to our attention that there were errors in Table 4 as regards the Right Ascension of the candidate coordinates. Table 4 should read as follows. This has no impact on the scientific results presented in the paper.

Table 4 Name, coordinates, Z, I, J, H and K magnitudes for our members to the cluster. The errors quoted are internal (from photon counting). The systematic calibration errors are 2% in the J, H and K wavebands (Warren et al., 2007), and 3% in the I and Z wavebands. The J, H and K magnitudes are on the MKO system. Previously discovered members also have their other known names listed from Moraux et al. (2003), Bihain et al. (2006) and Bouvier et al. (1998). The H and K band magnitudes are taken from the UKIDSS Galactic Cluster Survey with the exceptions of PLZJ 23, 93, 721 and 235 which have their H band magnitudes listed from our H survey. The K band magnitude for PLZJ 93 is from our UFTI photometry, and PLZJ 23 is from LIRIS service time. The final 5 objects in the table are our candidates selected from the ZJ data only.

Name	Alternate name	RA J2000.0	dec	$\mu_\alpha \cos\delta$ mas yr $^{-1}$	μ_δ	I	Z	J	H	K
PLZJ 29	BRB4	03 44 23.23	+25 38 45.11	23.40 \pm 8.24	-48.51 \pm 6.34	17.005 \pm 0.001	16.163 \pm 0.001	14.732 \pm 0.001	14.132 \pm 0.004	13.744 \pm 0.004
PLZJ 56		03 44 53.51	+25 36 19.46	19.68 \pm 7.34	-35.63 \pm 5.29	17.012 \pm 0.001	16.351 \pm 0.001	15.250 \pm 0.001	14.650 \pm 0.005	14.342 \pm 0.006
PLZJ 45	BRB8, CFHT-PL-7	03 52 05.82	+24 17 31.57	19.72 \pm 4.95	-42.37 \pm 7.44	17.101 \pm 0.001	16.417 \pm 0.001	15.247 \pm 0.001	14.614 \pm 0.005	14.251 \pm 0.006
PLZJ 50		03 43 55.98	+25 36 25.45	13.48 \pm 8.24	-35.65 \pm 5.38	17.239 \pm 0.001	16.496 \pm 0.001	15.268 \pm 0.001	14.693 \pm 0.006	14.319 \pm 0.006
PLZJ 60	CFHT-PL-10	03 44 32.32	+25 25 18.06	16.93 \pm 7.76	-43.15 \pm 5.72	17.592 \pm 0.001	16.810 \pm 0.001	15.460 \pm 0.001	14.884 \pm 0.007	14.465 \pm 0.006
PLZJ 78	PLIZ2	03 55 23.07	+24 49 05.18	19.72 \pm 10.06	-29.74 \pm 10.45	17.719 \pm 0.001	16.948 \pm 0.001	15.574 \pm 0.001	14.963 \pm 0.007	14.552 \pm 0.007
PLZJ 46	PLIZ3, BRB11	03 52 06.71	+24 16 00.99	19.55 \pm 5.15	-42.58 \pm 7.57	17.742 \pm 0.001	16.945 \pm 0.001	15.583 \pm 0.001	14.966 \pm 0.007	14.503 \pm 0.008
PLZJ 9	PLIZ6, BRB9	03 53 55.09	+23 23 36.38	24.13 \pm 13.83	-50.10 \pm 22.71	17.752 \pm 0.001	16.804 \pm 0.001	15.222 \pm 0.001	14.548 \pm 0.005	14.054 \pm 0.005
PLZJ 11	PLIZ20	03 54 05.33	+23 33 59.71	9.14 \pm 11.06	-28.98 \pm 11.94	19.571 \pm 0.004	18.563 \pm 0.004	16.691 \pm 0.005	15.980 \pm 0.016	15.436 \pm 0.016
PLZJ 77	PLIZ28, BRB18	03 54 14.04	+23 17 52.28	12.01 \pm 14.59	-51.60 \pm 15.84	20.760 \pm 0.010	19.728 \pm 0.010	17.647 \pm 0.010	16.789 \pm 0.031	16.131 \pm 0.030
PLZJ 21	PLIZ31	03 51 47.65	+24 39 59.18	17.84 \pm 9.41	-44.92 \pm 8.03	20.944 \pm 0.014	19.762 \pm 0.013	17.575 \pm 0.012	16.774 \pm 0.026	16.089 \pm 0.028
PLZJ 10	PLIZ35, BRB15	03 52 39.13	+24 46 29.61	15.84 \pm 8.88	-49.34 \pm 6.24	21.293 \pm 0.018	20.292 \pm 0.016	18.181 \pm 0.022	17.118 \pm 0.041	16.506 \pm 0.0416
PLZJ 4	BRB21	03 54 10.25	+23 41 40.67	29.74 \pm 13.17	-38.46 \pm 8.88	21.322 \pm 0.010	20.215 \pm 0.013	18.171 \pm 0.010	17.141 \pm 0.045	16.377 \pm 0.039
PLZJ 61	BRB22	03 44 31.27	+25 35 14.97	25.82 \pm 7.89	-40.21 \pm 8.47	22.043 \pm 0.030	20.782 \pm 0.026	18.298 \pm 0.020	17.393 \pm 0.059	16.657 \pm 0.04
PLZJ 32	BRB27	03 44 27.27	+25 44 41.99	25.03 \pm 11.52	-38.65 \pm 23.46	22.235 \pm 0.040	20.962 \pm 0.029	18.871 \pm 0.030	17.793 \pm 0.094	16.950 \pm 0.070
PLZJ 37	BRB28	03 52 54.92	+24 37 18.85	18.13 \pm 11.53	-48.68 \pm 11.38	22.452 \pm 0.05	21.216 \pm 0.041	18.839 \pm 0.030	17.742 \pm 0.071	16.921 \pm 0.058
PLZJ 23		03 51 53.38	+24 38 12.11	20.75 \pm 10.51	-50.05 \pm 9.96	23.541 \pm 0.140	22.187 \pm 0.112	19.960 \pm 0.100	19.362 \pm 0.100	18.510 \pm 0.030
PLZJ 93		03 55 13.00	+24 36 15.8	13.11 \pm 14.36	-33.77 \pm 12.97	24.488 \pm 0.370	22.592 \pm 0.164	19.968 \pm 0.080	19.955 \pm 0.100	19.420 \pm 0.100
PLZJ 323		03 43 55.27	+25 43 26.2	29.87 \pm 12.05	-39.37 \pm 11.70	-	21.597 \pm 0.054	19.613 \pm 0.076	-	-
PLZJ 721		03 55 07.14	+24 57 22.34	19.18 \pm 22.23	-40.70 \pm 12.38	-	22.195 \pm 0.092	20.248 \pm 0.116	20.417 \pm 0.123	-
PLZJ 235		03 52 32.57	+24 44 36.64	20.92 \pm 12.16	-45.84 \pm 11.75	-	22.339 \pm 0.115	20.039 \pm 0.112	20.245 \pm 0.127	-
PLZJ 112		03 53 19.37	+24 53 31.85	8.56 \pm 14.08	-34.59 \pm 19.99	-	22.532 \pm 0.116	20.281 \pm 0.143	-	-
PLZJ 100		03 47 19.19	+25 20 53.3	20.23 \pm 14.27	-37.28 \pm 23.82	-	23.563 \pm 0.373	20.254 \pm 0.114	-	-